Regular Paper

Biochemistry

Hoop-like role of the cytosolic interface helix in *Vibrio* PomA, an ion-conducting membrane protein, in the bacterial flagellar motor

Tatsuro Nishikino[1#], Yugo Sagara[2#], Hiroyuki Terashima[2, 3], Michio Homma[2]* and Seiji Kojima[2]*

[1]Institute for protein research, Osaka University, 3-2 Yamadaoka, Suita, Osaka, 565-0871, Japan; [2]Division of Biological Science, Graduate School of Science, Nagoya University, Chikusa-ku, Nagoya 464-8602, Japan; [3]Department of bacteriology, Institute of Tropical Medicine (NEKKEN), Nagasaki University, 1-12-4 Sakamoto, Nagasaki 852-8523, Japan

*Corresponding author: Division of Biological Science, Graduate School of Science, Nagoya University, Chikusa-ku, Nagoya 464-8602, Japan. Phone: +81-52-789-2993, Fax: +81-52-789-3054, E mail address: g44416a@cc.nagoya-u.ac.jp (to M.H.) and z47616a@cc.nagoya-u.ac.jp (S.K.).

[#]Both authors contributed equally to this work.

Running title: Cytosolic interface (CI) helix of PomA

Keywords: bacterial flagellum, stator, supramolecular complex, MotA, MotB

Author contributions: Y.S., S.K., and M.H. designed the research study; Y.S., T.N., H.T., M.H., and S.K. performed the experiments; Y.S., T.N., and S.K. analyzed the data; S.K. and M.H. wrote the paper.

Abstract

Vibrio has a polar flagellum driven by sodium ions for swimming. The force-generating stator unit consists of PomA and PomB. PomA contains four-transmembrane regions and a cytoplasmic domain of approximately 100 residues which interacts with the rotor protein, FliG, to be important for the force generation of rotation. The three-dimensional structure of the stator shows that the cytosolic interface (CI) helix of PomA is located parallel to the inner membrane. In this study, we investigated the function of CI helix and its role as stator. Systematic proline mutagenesis showed that residues K64, F66, and M67 were important for this function. The mutant stators did not assemble around the rotor. Moreover, the growth defect caused by PomB plug deletion was suppressed by these mutations. We speculate that the mutations affect the structure of the helices extending from TM3 and TM4 and reduce the structural stability of the stator complex. This study suggests that the helices parallel to the inner membrane play important roles in various processes, such as the hoop-like function in securing the stability of the stator complex and the ion conduction pathway, which may lead to the elucidation of the ion permeation and assembly mechanism of the stator.

47

48

49 **Introduction**

50

51 Most motile bacteria have filamentous macromolecular machine called flagella that extend
52 outside the cell and rotate like a screw to move to a favorable environment for survival. An
53 ion-driven rotary motor consists of a stator and a rotor at the base of the flagella. The stator
54 converts the electrochemical potential difference between the inside and outside the cell into a
55 torque that is generated by interaction with the rotor. The coupling ions that drive the flagellar
56 motor are known to be protons (H^+) in *Escherichia coli* and *Salmonella*, or sodium ions (Na^+)
57 in *Vibrio* species and alkalophilic *Bacillus* (1-3).

58 The stator is composed of MotA and MotB in *E. coli* and *Salmonella*, and the
59 orthologs PomA and PomB in *Vibrio*. PomA (MotA) is a four-transmembrane (TM) protein
60 with a large cytoplasmic loop ($Loop_{2-3}$) between the second and third TM regions. The $loop_{2-3}$
61 contains several conserved charged residues, and the electrostatic interactions between these
62 residues and the conserved charged residues of FliG of the rotor are important for motor
63 rotation (4-7). PomB (MotB) is a single TM protein and the TM region is present in the N-
64 terminus and the C-terminal region is present in the periplasmic space (8, 9) In the
65 periplasmic region of PomB (MotB), there is an OmpA-like domain responsible for

66 peptidoglycan binding (PGB), which anchors the stator to the peptidoglycan layer around the
67 rotor via a PGB motif and the PGB region of Pal is interchangeable with the PGB region of
68 MotB (10, 11). The crystal structures of the PGB region have already been solved (12-14),
69 and it has been speculated that the structure changes significantly when the stator unit is
70 activated, allowing it to be assembled and anchored around the rotor periphery (15). A
71 segment of approximately 15 residues, called the plug region adjacent to the MotB or PomB
72 TM region, prevents the ion influx of the stator as when the stator does not assemble around
73 the rotor (16-18).

74 The structure of the cytoplasmic loop ($Loop_{2-3}$) of the stator PomA (MotA)
75 interacting with the rotor (FliG) is very important for the mechanism of torque generation (5,
76 6). The interaction between the PomA cytoplasmic loop and the FliG C-terminal region was
77 directly detected by the site-directed photo-crosslinking between the residues of PomA D85,
78 R88, K89, G90, F92, L93, or E96 and the residues of the FliG C-terminal region (19). We
79 have previously attempted to clarify the structure of $Loop_{2-3}$ by preparing various constructs.
80 However, they all precipitated when overexpressed in *E. coli*, and we could not proceed to the
81 structural analysis (20). Thus, we predicted the structure of PomA based on the structure of
82 ExbB, whose structures have been reported in *E. coli* (21, 22) and showed weak amino acid
83 sequence similarity to PomA. Furthermore, ExbB is a membrane protein complex responsible
84 for energy conversion using an ion-driven force and has an operating mechanism similar to

that of PomA. Based on the ExbB atomic structure, we predicted the stator structure composed of PomA and PomB, and Pro-substituted mutants were constructed in $Loop_{2\text{-}3}$. In 2020, the structures of MotAB stator derived from *Campylobacter jejuni*, *Clostridium sporogenes*, and *Bacillus subtilis* were determined by single-particle analysis using cryo-electron microscopy (23-25). The MotA/MotB and PomA/PomB complexes, previously proposed as 4:2 hetero-hexamers, were shown to be 5:2 hetero-heptamers. From the structure in which two molecules of MotB are inserted in the center of the MotA ring made of five molecules, a model was proposed in which the MotA ring rotates with respect to the axis of MotB due to the influx of ions. It has been recently suggested that the plug region functions as a "spanner" to prevent the stator PomA pentamer ring rotation around the PomB TM axis, so that the ion flux and the stator rotation are coupled (26).

In this study, we focused on the characteristic cytosolic interface (CI) helix parallel to the inner membrane interface in $Loop_{2\text{-}3}$. To investigate the roles of this helix in the stator function, we made Pro and other amino acid substitutions in the CI helix of PomA.

Materials and Methods

Bacterial strains and plasmids

104 *E. coli* was cultured in LB broth [1% (w/v) bactotryptone, 0.5% (w/v) yeast extract, and 0.5%
105 (w/v) sodium chloride (NaCl)], LB 3% NaCl broth [1% (w/v) bactotryptone, 0.5% (w/v) yeast
106 extract, and 3% (w/v) NaCl], and TG broth [1% (w/v) bactotryptone, 0.5% (w/v) NaCl, and
107 0.5% (w/v) glycerol). Chloramphenicol was added at a final concentration of 25 μg/mL for *E.*
108 *coli*. Ampicillin was added at a final concentration of 100 μg/mL for *E. coli*. *V. alginolyticus*
109 was cultured at 30 °C in VC medium [0.5% (w/v) polypeptone, 0.5% (w/v) yeast extract,
110 0.4% (w/v) K_2HPO_4, 3% (w/v) NaCl, and 0.2% (w/v) glucose) or VPG medium [1% (w/v)
111 polypeptone, 0.4% (w/v) K_2HPO_4, 3% (w/v) NaCl, and 0.5% (w/v) glycerol]. If needed,
112 chloramphenicol was added at a final concentration of 2.5 μg/mL for *V. alginolyticus* culture.
113
114 **Mutagenesis**
115 Site-directed mutagenesis was performed using the QuikChange site-directed mutagenesis
116 method, as described by Agilent Technologies (Santa Clara, USA). Transformations of *V.*
117 *alginolyticus* by pHFAB and the mutant derivative plasmids or of *E. coli* by pCold4
118 derivative plasmids were carried out by electroporation as described previously (27).
119
120 **Disulfide crosslinking experiment**
121 Cells harboring the pHFAB plasmids were cultured in the VPG medium containing arabinose
122 at a final concentration of 0.02% (w/v) at 30 °C for 4 h with 100-fold dilution from the

123 overnight culture. To examine disulfide crosslinking, the cells were collected by
124 centrifugation and then suspended in SDS-loading buffer without β-mercaptoethanol. SDS-
125 PAGE and immunoblotting were performed as previously described (26).
126
127 **Swimming assay in soft agar plates**
128 *Vibrio* NMB191 cells harboring the pHFAB-based plasmids with the mutants or wild-type
129 *pomA* and *pomB* were plated on VPG plates with antibiotics. A colony of *Vibrio* cells was
130 inoculated onto VPG agar [0.25% (w/v) bactoagar] plates containing 0.02% (w/v) arabinose
131 and incubated at 30 °C.
132
133 **Purification of PomAB complex**
134 The purification protocols were modified as previously described (27). BL21 (DE3) cells
135 carrying the plasmid pCold4 *pomApomB-his*$_6$ which had been previously constructed (27),
136 and pLysS were grown overnight in 30 mL of LB medium at 37 °C, inoculated in 1.5 L of LB
137 medium, and incubated at 37 °C. When the cell density at OD_{660nm} approximately reached 0.4,
138 cells were incubated in iced water for 30 min. Isopropyl β-D-1-thiogalactopyranoside (IPTG)
139 was added to a final concentration of 0.5 mM to induce overexpression of PomA and PomB-
140 His$_6$ proteins and cultured for 1 d at 15 °C. Cells were harvested by centrifugation and the
141 weight of the cells was measured. Seven times the volume of Na-Pi buffer (50 mM Na-Pi pH

8.0, and 200 mM NaCl) was added and the cells were suspended. To break the cells, the suspension was placed in a French press (OHTAKE) at 1,000 kg/cm^2. Unbroken cells were removed by low-speed centrifugation. The samples were ultra-centrifuged at 118,000 × *g* for 1 h. The same volume of Na-Pi buffer before the French press was added to the resultant pellet and stored at –30 °C for later use. The frozen samples (10 mL and 40 mL volume) in the WT and mutants, respectively, were thawed in a water bath and stirred. To solubilize the resultant pellet, 10% (w/v) DMNG was added to a final concentration of 0.5% (w/v) and stirred for 60 min at 30 °C. The insoluble material was removed by ultra-centrifugation (118,100 × *g* for 30 min). The resultant supernatant was mixed with 4 mg of Talon Metal Affinity Resin (Takara) equilibrated with wash buffer [50 mM Na-Pi pH 8.0, 200 mM NaCl, 10 mM imidazole, and 0.02% (w/v) DMNG) and incubated at 4 °C for at least 1 h in a polypropylene column by batch method. After eluting the supernatant in the column, 4 mL (1 column volume) of wash buffer was added to the column three times to wash the column. To elute the His-tag stator from the resin, two column volumes of elution buffer [50 mM Na-Pi (pH 8.0), 200 mM NaCl, 200 mM imidazole, and 0.02 % (w/v) DMNG] was added and eluted. The his-tag affinity purified stator was concentrated to 1 ml using a 100 K MWCO Amicon device (Millipore). The samples were subjected to size exclusion chromatography using Enrich SEC650 column (Bio rad) in SEC buffer [20 mM Tris HCl (pH8.0), 100 mM KCl and 0.0025% (w/v) 2,2-didecylpropane-1,3-bis-β-D-maltopyranoside (LMNG)]. We set

the flow at 0.75 mL per min and fraction volume of elution at 0.5 mL. The peak fractions were collected, and the concentrations were measured by absorptiometry (ε= 50310) of A280 using a Nanodrop (Thermo Scientific).

Sample preparation and data correction of negative staining images

Elution fractions of WT and PomA-F66S mutations were diluted in SEC buffer. Final concentration of the samples in the WT and F66S mutation were 3.4 and 5.3 ng/mL, respectively. A 5 μL solution was applied to a glow-discharged continuous carbon grid. The excess solution was removed using filter paper, and the sample was subsequently stained on the carbon grid with 2% ammonium molybdate. Electron microscopy images were recorded with an H-7650 transmission electron microscope (Hitachi) operated at 80 kV and equipped with a FastScan-F114 CCD camera (TVIPS, Gauting, Germany) at a nominal magnification of 80,000 ×.

Protein structural analysis

The protein structural analysis and drawing were performed using a software, MolFeat (FiaLux co., Japan).

Results

Motility and protein expression of the Pro mutants

We predicted the secondary structure of PomA based on the structure of ExbB (22, 28), which showed homology to PomA, and introduced proline replacements, a predicted helix breaker, into the residues of the helix that follow the TM2 helix (G53 to A70) in the PomA $Loop_{2\text{-}3}$ region (Fig. 1A). While we had introduced the mutations and analysis the mutants, the stator structures were reported by single-particle analysis using cryo-electron microscopy (23, 25). Thus, we realized that the mutations were introduced in the CI helix of $Loop_{2\text{-}3}$ parallel to the inner membrane (Fig. 1B and 1C). Plasmids expressing Pro-substituted PomA and wild-type (WT) PomB were introduced into NMB191 (*pomAB*-deficient strain) and expressed by arabinose induction. Motility was evaluated by swimming ring formation on a soft agar. The K60P, K64P, F66P, and M67P mutants showed no swimming ring formation, and the lack of motility was confirmed by light microscopy (Fig. 2A). The protein expression of each mutant was detected by western blotting using an anti-PomA antibody (PomA1312) which is raised by a peptide fragment (P231-E253 of PomA). All mutants, except for the K60P mutation, produced PomA (Fig. 2B). It is noteworthy that most mutant PomA bands were detected as a single band (ca. 25 kDa by SDS-PAGE) in western blotting, whereas the WT PomA was

198 detected as a double band in which ca. 25 kDa and ca. 26 kDa bands were detected. This
199 suggests that these mutations affect the structure of PomA.
200
201 **Motility of Ala and Ser mutants and dominant effects of the mutants**
202 To investigate the residue specificity of the Pro substitutions, we replaced the residues K64,
203 F66, and M67 with Ala or Ser. The motility assay on soft agar showed that the motility of
204 F66A, M67A, and M67S was similar to that of the WT, and that of the K64A mutant was
205 reduced, while that of the K64S and F66S mutants was completely lost (Fig. 3A). We
206 speculate that the M67P mutation might affect the structure of the F66 residue, which is the
207 neighbor of M67. Protein expression of each mutant was detected by western blotting using
208 an anti-PomA antibody, and protein expression was confirmed in all mutants (Fig. 3C).
209 Next, we examined the dominance of these mutants. A plasmid expressing the
210 mutant PomA was introduced into the WT VIO5 strain of the polar flagellar motor, and
211 PomA mutant expression was induced by arabinose. The plasmid-derived mutant PomA was
212 expressed more than the chromosome-derived WT PomA. The dominant effects of Pro and
213 Ser mutants were not observed (Fig. 3B and 3D).
214
215 **Analysis of stator function**

The lack of the dominant effect of the mutant PomA suggests that the mutant stator complex is not able to assemble around the rotor. To examine whether Pro-substituted PomA does not assemble around the rotor, we expressed the mutant GFP-fused PomB with PomA from a plasmid in NMB191 (*pomAB*-deficient strain) by induction of arabinose. When WT PomA and GFP-fused PomB were expressed, fluorescence dots were observed at the poles of cells, indicating that the PomAB complex was assembled around the motor (Fig. 4A). On the other hand, almost no fluorescent dots could be observed in the PomA-K64P and F66S mutants, indicating that the PomAB complex cannot assemble around the rotor.

Although the loss of motility by the Pro mutation was explained by the inability of stator assembly around the rotor, we examined whether the mutant PomA with PomB, itself, is functional, that is, whether the mutant PomAB complex is capable of ion permeation. The plug region (residues 44-58) in PomB acts as a lid to prevent ion flow from the extracellular region. When the plug mutant ($PomB_{\Delta L}$) is expressed in *E. coli* cells, excessive ion influx by the stator inhibits cell growth. When mutant PomA and PomB deficient in the plug region were co-expressed from a plasmid in *E. coli* DH5α by arabinose induction, growth inhibition was suppressed by the K64P and F66S mutations (Fig. 4B) and we confirmed the PomA expression (Fig. S1). This suggests that the K64P and F66S mutations affect the structure of the ion channel. We speculated that inhibition of ion flux in the stator by the mutations prevented the stator from anchoring the stator around the rotor.

Purification of stator complex

We have improved the purification of the PomAB stator complex by using a cold-shock vector overexpression system in *E. coli* and the detergent, decyl maltose neopentyl glycol (DMNG), and have been able to obtain a reproducible, stable, and highly pure purified complex (27). We purified the PomAB stator with PomA F66S and K64P mutations. We could purify the mutant stator similar to the WT, although the amount of both mutants was reduced. After affinity chromatography and Coomassie brilliant blue (CBB) staining of the purified sample, bands of PomA and PomB were observed, confirming the formation of the complex. The affinity chromatography sample was then concentrated, and gel filtration chromatography was performed using a diluted sample of WT (Fig. 5A). F66S, and K64P stator were eluted at peak volumes of 11.19 mL and 11.33 mL, respectively, which are close to the WT peak volume of 11.26 mL. We estimated molecular weight the major peaks of them, and that of WT, K64P and F66S mutants were 320 kDa, 300 kDa and 340 kDa, respectively, corresponding to the molecular weight of the stator (210 kDa) with detergent micelles. It is noteworthy that the F66S and K64P complexes eluted with a shoulder at peak volumes of 9.90 ml and 9.26 ml, and molecular weight of them were 1,500 kDa and 900 kDa, respectively, estimating as the void. We do not know the reason why the elution profiles are slightly different compared to the WT, although we speculate that the binding number of detergents is different and the stator complex was unstable with the mutation. To confirm the

254 stator structure of the purified stator, we observed the stator by electron microscopy (Fig. S2).
255 The particles of the stator were observed, and we could not find any notable differences in
256 particle shapes between the WT. Detailed structural analysis by cryo-electron microscopy is
257 currently in progress.
258
259 **The cross-link formation between PomA TM1 and TM2**
260 The CI helix lies between TM1 and TM2 and beneath the inner membrane and is located
261 outside the pentamer as if each of it encircles a PomA molecule to hold the whole pentamer
262 ring. Thus, we speculated that the CI helix might stabilize the molecules of PomA in the
263 pentamer, and mutations in the CI region may destabilize the PomA structure, thereby losing
264 the stator function. We investigated the residue pair of adjacent PomA molecules in the
265 pentamer ring that are located at different distances to form a disulfide bridge when the
266 residues are substituted with Cys (Fig. 6). We found that PomA with L22C and T33C
267 mutations, which are close to each other in the pentamer ring, form multimers and appear to
268 be up to pentamer, as judged by western blotting (Fig. 6A). Since the PomA-L22C/T33C
269 mutant showed only slightly reduced motility compared to the WT or mutants with a single
270 mutation in the soft agar plate (Fig. 6B), the stator function was not significantly affected by
271 the disulfide cross-link. We expected that if the disulfide cross-link could stabilize the TM
272 helices in the stator, then the function of the K66P or F66S mutant stator would be restored.

We introduced the K64P and F66S mutations in the L22C and T33C mutant PomA. The disulfide cross-linking did not suppress the K64P and F66S mutations (Fig. 6D). The K64P and F66S mutations did not affect disulfide cross-link formation, suggesting that the structures of TM1 and TM2 were not affected by the K64P and F66S mutations (Fig. 6C).

Discussion

The flagellum is the locomotor machinery of many bacteria, including marine species belonging to the genus *Vibrio*. The rotational force is generated by the interaction between the stator and rotor via the ion flow in the stator. The interaction between the cytoplasmic region of $Loop_{2\text{-}3}$ in the A subunit and the C-terminal region of the rotor protein of FliG is important for torque generation. We attempted to obtain the structural information of the $Loop_{2\text{-}3}$ region, which is unknown. Last year, the three-dimensional structure of the stator complex (MotAB) from *Campylobacter jejuni*, *Clostridium sporogenes*, and *Bacillus subtilis* had been clarified (23, 25). We studied the sodium-driven flagellar motor of marine *Vibrio*, *Vibrio alginolyticus*. In this study, we systematically constructed proline-substituted mutants (from G53 to A70) in the cytoplasmic region close to TM2 in PomA. When the structure of MotA, which had been determined, was assigned to the corresponding structure and sequence of PomA, the Pro

292 mutations were located in the CI helix, which is parallel to the inner membrane boundary
293 (Fig. 1).
294 Among the 28 proline mutants, only three mutants (K64P, F66P, and M67P) were
295 found to lose motility, even though the Pro mutant PomA proteins were expressed. These
296 three residues (K64, F66, and M67) are localized in the C-terminal site of the CI helix, which
297 is parallel to the inner membrane interface. To examine the effects of other amino acid
298 substitutions, we introduced Ala or Ser into the residues K64, F66, and M67 (Fig. 3). We
299 found that in the K64 residue, the Ala and Ser mutations reduced and lost motility,
300 respectively, suggesting that the electrostatic interaction of this residue might be required for
301 ion flux. In the F66 residue, the Ala and Ser mutations resulted in normal motility and loss of
302 motility (Fig. 3 and S3), respectively. Hydrophobicity or α-helix formation by this residue
303 may be important for stator function. Other mutations did not affect motility. The WT PomA
304 band by sodium dodecyl sulfate-polyacrylamide gel (SDS-PAGE) was detected as double-
305 banded, suggesting that distinct stable structures were present even in the solution containing
306 the strong detergent SDS. Most proline mutants of PomA in the CI helix become single-
307 banded. This region may contribute to the stability of monomer PomA; however, the
308 character of the monomer stability does not seem to correlate with the stator functions.
309 According to the dominant effect and the ability of poler localization of the stator
310 complex, it seems that the CI mutant stators, which lost their function, could not assemble

311 around the rotor (Fig. 4A). The stator assembly around the motor is necessary for activation
312 and interaction with the peptidoglycan (PG) layer or T-ring depending on Na^+ ions or
313 interaction with FliG (29-32). The mutations may have altered the structure of the stator
314 complex to prevent the sensing of Na^+, thus inhibiting the interaction with the rotor. Next, we
315 tested whether the stator could permeate ions in the growth assay using PomB lacking the
316 plug region. PomA mutations suppressed growth inhibition (Fig. 4B), indicating that these
317 mutations prevent ion flux. In other words, the structural instability caused by the mutations
318 may abolish the rotor-stator interaction and block the Na^+-conductive activity induced by the
319 stator activation due to the interaction with the rotor. We have not yet clarified whether the
320 mutation actually inhibits the ion permeation pathway or what kind of structural changes are
321 induced by the mutations. Although the ion permeation pathway has not been clarified, the
322 third and fourth TM regions of PomA and the TM region of PomB are thought to form the ion
323 pathway, the PomB-D24 residue in the TM region and PomA-T158 and PomA-T186, which
324 are located in TM3 and TM4, respectively, are known to be the essential Na^+ binding sites
325 (27, 33). Structural alteration at the C-terminal side of the CI helix may affect the structure of
326 the Na^+-binding site composed of these residues, although the overall structure of the stator
327 complex was not altered by the mutations, as judged by gel-filtration chromatography of
328 purified mutant stators (Fig. 5). It should be noted that the amount of expression was lower

than that of the WT, and the shape of the gel filtration chromatography peaks did not allow us to conclude that this was due to structural differences.

The CI helix parallel to the inner membrane interface contains a large number of hydrophobic residues, suggesting that the hydrophobic profile of this helix serves as a CI helix. The F66 residue is highly conserved among the residues of the CI helix (Fig. 1A) and is likely to play an important role. Since the F66 residue is a hydrophobic residue with an inward-facing side chain, it may stabilize the structure through hydrophobic interactions with the other helices. The K64 residue is predicted to be exposed on the surface of the stator complex (Fig. 7 and S4). The K64 residue is a charged residue, and the electrostatic map of the stator complex (Fig. 7A) shows that the boundary region to the inner membrane, where the K64 residue is located, is positively charged, and the membrane, which composed of phospholipids, is negatively charged. This suggests that the K64 residue is involved in the stability of the stator through electrostatic interaction with the inner membrane, or is involved in the stabilization of the structure by interacting with charged residues in the helix extending from TM3 and TM4. In accordance with this assumption, the K203 residue, which is located at the C-terminal end of TM4 and structurally close to the K64 residue (Fig. 7C), is known to lose its motility due to the K203E mutation (34), suggesting that charged residues near the CI helix are important for stator function. The amino acid sequences of the CI region are not highly homologous among the species, although many positively charged amino acids are

present in the CI region and the CI helix are similarly arranged in the stator structures (Fig. S5). The surface charges of CI helix in *C. sporogenes* seems to be different from the others, *C. jejuni* and *B. subtilis*. This different may be derived from that *C. sporogenes* is anaerobic bacterium and its membrane property is different from the others. Based on our results, we propose that the CI helix, which lies parallel to the inner membrane, has a hoop-like function to support the TM3 and TM4 helices, which extend to the ion binding site. Interaction with the membrane surface with CI helices stabilizes the stator complex and ion-conducting pathway.

Acknowledgements

This work was supported in part by the Japan Society for the Promotion of Science (JSPS) KAKENHI [Grant Numbers 18K07108 and 21K07022 (to H.T.), A20J00329 (to T.N.), and 20H03220 (to M.H.)].

Supporting information

Supplementary information associated with this article can be found online on the publisher's website.

References

1. Blair D.F. (2003) Flagellar movement driven by proton translocation. *FEBS Lett.* **545**, 86-95.
2. Takekawa, N., Imada, K., and Homma, M. (2020) Structure and energy-conversion mechanism of bacterial Na^+-driven flagellar motor. *Trends Microbiol.* **28**, 719-731.
3. Terashima, H., Kojima, S., and Homma, M. (2008) Flagellar motility in bacteria structure and function of flagellar motor. *Int. Rev. Cell Mol. Biol.* **270**, 39-85.
4. Onoue, Y., Takekawa, N. Nishikino, T., Kojima, S., and Homma, M. (2018) The role of conserved charged residues in the bidirectional rotation of the bacterial flagellar motor. *Microbiologyopen* 7:e00587.
5. Takekawa, N., Kojima, S., and Homma, M. (2014) Contribution of many charged residues at the stator-rotor interface of the Na^+-driven flagellar motor to torque generation in *Vibrio alginolyticus*. *J. Bacteriol.* **196**, 1377-1385.
6. Yakushi, T., Yang, J., Fukuoka, H., Homma, M., and Blair, D.F. (2006) Roles of charged residues of rotor and stator in flagellar rotation: comparative study using H^+-driven and Na^+-driven motors in *Escherichia coli*. *J. Bacteriol.* **188**, 1466-1472.

386 7. Zhou, J., Sharp, L.L., Tang, H.L., Lloyd, S.A., Billings, S., Braun, T.F., and Blair, D.F.
387 (1998) Function of protonatable residues in the flagellar motor of *Escherichia coli*: a
388 critical role for Asp 32 of MotB. *J. Bacteriol.* **180**, 2729-2735.
389 8. Asai, Y., Kojima, S., Kato, H., Nishioka, N., Kawagishi, I., and Homma, M. (1997)
390 Putative channel components for the fast-rotating sodium-driven flagellar motor of a
391 marine bacterium. *J. Bacteriol.* **179**,5104-5110.
392 9. Chun, S.Y., and Parkinson, J.S. (1988) Bacterial motility: membrane topology of the
393 *Escherichia coli* MotB protein. *Science* **239**, 276-278.
394 10. De Mot, R., and Vanderleyden, J. (1994) The C-terminal sequence conservation between
395 OmpA-related outer membrane proteins and MotB suggests a common function in both
396 gram- positive and gram-negative bacteria, possibly in the interaction of these domains
397 with peptidoglycan. *Mol. Microbiol.* **12**, 333-334.
398 11. Hizukuri, Y., Morton, J.F., Yakushi, T., Kojima, S., and Homma, M. **(**2009) The
399 peptidoglycan-binding (PGB) domain of the *Escherichia coli* Pal protein can also
400 function as the PGB domain in *E. coli* flagellar motor protein MotB. *J. Biochem.* **146**,
401 219-229.
402 12. Kojima, S., Imada, K., Sakuma, M., Sudo, Y., Kojima, C., Minamino, T., Homma, M.,
403 and Namba, K. (2009) Stator assembly and activation mechanism of the flagellar motor
404 by the periplasmic region of MotB. *Mol. Microbiol.* **73**, 710-718.

13. Roujeinikova, A. (2008) Crystal structure of the cell wall anchor domain of MotB, a stator component of the bacterial flagellar motor: implications for peptidoglycan recognition. *Proc. Natl. Acad. Sci. USA.* 105: 10348-10353.

14. Zhu, S., Takao, M., Li, N., Sakuma, M., Nishino, Y., Homma, M., Kojima, S., and Imada, K. (2014) Conformational change in the periplamic region of the flagellar stator coupled with the assembly around the rotor. *Proc. Natl. Acad. Sci. USA.* **111**, 13523-13528.

15. Kojima, S., Takao, M., Almira, G., Kawahara, I., Sakuma, M., Homma, M., Kojima, C., and Imada, K. (2018). The helix rearrangement in the periplasmic domain of the flagellar stator B subunit activates peptidoglycan binding and ion influx. *Structure* **26**, 590-598.

16. Hosking, E.R., Vogt, C., Bakker, E.P., and Manson, M.D. (2006) The *Escherichia coli* MotAB proton channel unplugged. *J. Mol. Biol.* **364**, 921-937.

17. Li, N., Kojima, S., and Homma, M. (2011) Characterization of the periplasmic region of PomB, a Na^+-driven flagellar stator protein in *Vibrio alginolyticus*. *J. Bacteriol.* **193**, 3773-3784.

18. Takekawa, N., Terauchi, T., Morimoto, Y.V., Minamino, T., Lo, C.J., Kojima, S., and Homma, M. (2013) Na^+ conductivity of the Na^+-driven flagellar motor complex composed of unplugged wild-type or mutant PomB with PomA. *J. Biochem.* **153**, 441-451.

19. Terashima, H., Kojima, S., and Homma, M. (2021) Site-directed crosslinking identifies the stator-rotor interaction surfaces in a hybrid bacterial flagellar motor. *J. Bacteriol.* **203**, e00016-21.

20. Onoue, Y., Abe-Yoshizumi, R., Gohara, M., Kobayashi, S., Nishioka, N., Kojima, S., and Homma, M. (2014) Construction of functional fragments of the cytoplasmic loop with the C-terminal region of PomA, a stator component of the *Vibrio* Na^+ driven flagellar motor. *J. Biochem.* **155**, 207-216.

21. Celia, H., Botos, I., Ni, X., Fox, T., De Val, N., Lloubes, R., Jiang, J., and Buchanan, S.K. (2019) Cryo-EM structure of the bacterial Ton motor subcomplex ExbB-ExbD provides information on structure and stoichiometry. *Commun. Biol.* **2**, 358.

22. Maki-Yonekura, S., Matsuoka, R., Yamashita, Y., Shimizu, H., Tanaka, M., Iwabuki, F., and Yonekura, K. (2018) Hexameric and pentameric complexes of the ExbBD energizer in the Ton system. *eLife* **7**, e35419

23. Deme, J.C., Johnson, S., Vickery, O., Aron, A., Monkhouse, H., Griffiths, T., James, R.H., Berks, B.C., Coulton, J.W., Stansfeld, P.J., and Lea, S.M. (2020) Structures of the stator complex that drives rotation of the bacterial flagellum. *Nat. Microbiol.* **5**, 1553-1564.

24. Hu, H., Santiveri, M., Wadhwa, N., Berg, H.C., Erhardt, M., Taylor, N.M.I. (2021) Structural basis of torque generation in the bi-directional bacterial flagellar motor. *Trends*

443 *Biochem. Sci.* doi:10.1016/j.tibs.2021.06.005

444 25. Santiveri, M., Roa-Eguiara, A., Kühne, C., Wadhwa, N., Hu, H., Berg, H.C., Erhardt, M.,
445 Taylor, N.M.I. (2020) Structure and function of stator units of the bacterial flagellar
446 motor. *Cell* **183**, 244-257.

447 26. Homma, M., Terashima, H., Koiwa, H., and Kojima, S. (2021) Putative spanner function
448 of the *Vibrio* PomB plug region in the stator rotation model for flagellar motor. *J.*
449 *Bacteriol.* **203**, e00159-21.

450 27. Onoue, Y., Iwaki, M., Shinobu, A., Nishihara, Y., Iwatsuki, H., Terashima, H., Kitao, A.,
451 Kandori, H., and Homma, M. (2019) Essential ion binding residues for Na^+ flow in stator
452 complex of the *Vibrio* flagellar motor. *Sci. Rep.* **9**, 11216.

453 28. Celia, H., Noinaj, N., Zakharov, S.D., Bordignon, E., Botos, I., Santamaria, M., Barnard,
454 T.J., Cramer, W.A., Lloubes, R., and Buchanan, S.K. (2016) Structural insight into the
455 role of the Ton complex in energy transduction. *Nature* **538**, 60-65.

456 29. Fukuoka, H., Wada, T., Kojima, S., Ishijima, A., Homma, M. (2009) Sodium-dependent
457 dynamic assembly of membrane complexes in sodium-driven flagellar motors. *Mol.*
458 *Microbiol.* **71**, 825-835.

459 30. Kojima, S., Nonoyama, N., Takekawa, N., Fukuoka, H., Homma, M. (2011) Mutations
460 targeting the C-terminal domain of FliG can disrupt motor assembly in the Na^+-driven
461 flagella of *Vibrio alginolyticus*. *J. Mol. Biol.* **414**, 62-74.

462 31. Mino, T., Nishikino, T., Iwatsuki, H., Kojima, S., and Homma, M. (2019) Effect of
463 sodium ions on conformations of the cytoplasmic loop of the PomA stator protein of
464 *Vibrio alginolyticus*. *J. Biochem.* **166**, 331-341.
465 32. Terashima, H., Li, N., Sakuma, M., Koike, M., Kojima, S., Homma, M., and Imada, K.
466 (2013) Insight into the assembly mechanism in the supramolecular rings of the sodium-
467 driven *Vibrio* flagellar motor from the structure of FlgT. *Proc. Natl. Acad. Sci. USA.* **110**,
468 6133-6138.
469 33. Sudo, Y., Kitade, Y., Furutani, Y., Kojima, M., Kojima, S., Homma, M., and Kandori, H.
470 (2009) Interaction between Na^+ ion and carboxylates of the PomA-PomB stator unit
471 studied by ATR-FTIR spectroscopy. *Biochemistry* **48**, 11699-11705.
472 34. Obara, M., Yakushi, T., Kojima, S., and Homma, M. (2008) Roles of charged residues in
473 the C-terminal region of PomA, a stator component of the Na^+-driven flagellar motor. *J.*
474 *Bacteriol.* **190**, 3565-3571.
475
476
477 **Figure legends**
478
479 **Fig. 1.** (A) Alignment of the N-terminal sequences of the stator proteins, PomA and MotA.
480 The transmembrane region (TM) is shown in yellow. The mutated residues in the PomA of

Vibrio alginolyticus mutated in this study are shown in red. VaPomA: PomA of *Vibrio alginolyticus* VIO5 (wild-type strain for the polar flagellum), AaMotA: MotA of *Aquifex aeolicus*, TmMotA: MotA of *Thermotoga maritima*, VaMotA: MotA of *Vibrio alginolyticus* VIO5, EcMotA: MotA of *Escherichia coli*, and CjMotA: MotA of *Campylobacter jejuni*. (B, C, D) Atomic structure model of the *C. jejuni* (Cj) stator, MotAB (PDB ID: 6YKM). The MotB part corresponding to PomB, and the cytosolic interface (CI) region of MotA corresponding to PomA are shown in light blue and blue, respectively. The residues of MotA corresponding to K60, K64, F66, and M67 of PomA are shown by the ball-and-stick model in black. The residues of MotA corresponding to the putative interacting charged and hydrophobic residues PomA are shown by the space filling model in red and black, respectively. (B) Side view of the stator with the inner membrane which is indicated by a gray rectangle and (C) slanting view from the top. (D) The CI region is expanded from (B).

Fig. 2. The motility of Pro substitution mutant and its protein expression.

(A) *Vibrio* NMB191 (*pomAB* mutant) cells harboring the pHFAB-based plasmid with the *pomA* mutations from the fresh colonies were inoculated in soft agar plates (VPG 0.25%) with 0.02% arabinose and incubated at 30 ºC for 5 h. (B) *Vibrio pomAB* mutnat cells harboring the same pHFAB-based plasmid above with mutations were grown to the mid-log phase. The

proteins of the cells were then separated using sodium dodecyl sulfate-polyacrylamide gel (SDS-PAGE) and detected via western blotting using the anti-PomA antibody.

Fig. 3. Mutations other than Pro and the dominant effects caused by the mutants.

Vibrio pomAB (A) or wild-type (B) cells harboring the pHFAB-based plasmid without PomA (vector) or with wild-type PomA (WT) and the Ala and Ser substituted mutants (K64A, K64S, F66A, F66S, M67A, or M67S) from the fresh colonies were inoculated in soft agar plates (VPG 0.25%) with 0.02% arabinose and incubated at 30 °C for 5 h. *Vibrio pomAB* (C) or wild-type (D) cells harboring the same pHFAB-based plasmid above with the mutations were grown to the mid-log phase. The proteins of the cells were then separated using SDS-PAGE and detected by western blotting using an anti-PomA antibody.

Fig. 4. Profiles of the K64P and F66S mutants.

(A) *Vibrio pomAB* cells harboring the pHFGBA with wild-type PomA (WT) or K64P and F66S of PomA substituted mutants were cultured in VPG broth containing 0.02% arabinose for 4 h at 30 °C and were observed by fluorescent microscopy. (B) Growth curve of cells. Overnight culture of *E. coli* cells harboring pBAD33 (Vector) and pTSK37 (PomA/BΔL) and derivative plasmids (PomA-K64P/BΔL, and PomA-F66S/BΔL) was inoculated in the LB 3% sodium chloride (NaCl) broth at 1/100 dilution; arabinose was added at a final concentration

518 of 0.02% (w/v), 2 h later, to induce expression (arrow). A_{660} was measured every 1 h after

519 induction.

520

521 **Fig. 5. Profiles of the purified stator with the mutants in PomA.**

522 (A) Elution profile of the size exclusion chromatogram in the WT-stator complex and mutant.

523 The stator expressed in *E. coli* cells by pColdIV-*pomA-pomB-his6* plasmid with WT PomA,

524 K64P, or F66S mutation and purified by the affinity chromatography using hexa-histidine tag

525 was subjected to size exclusion chromatography. The peak elution fractions (approximately at

526 10 mL) in each sample are shown. The black arrows indicated in calibration makers. a, b, c

527 and d were 670 kDa Thyroglobulin, 440 kDa Ferritin, 158 kDa Bovine gamma globulin, and

528 44 kDa Chicken ovalbumin, respectively. (B) Proteins of WT-stator, stator with K64P

529 mutation in PomA, were purified and the elution samples by size exclusion chromatography

530 were analyzed by SDS-PAGE and stained with Coomassie brilliant blue (CBB). The peak

531 elution fractions (approximately at 10 mL) in each sample are shown.

532

533 **Fig. 6. Effect of the PomA mutations on cysteine-substituted mutants.**

534 (A) Proteins extracted from *Vibrio pomAB* cells harboring 1: pBAD33 (vec), 2: pHFAB

535 (WT), and pHFAB-based plasmid with the mutations, 3: *pomA-L22C* (L22C), 4: *pomA-T33C*

536 (T33C), and 5: *pomA-L22C*, *T33C* (L22C&T33C) were separated using SDS-PAGE in the

537 absence of a reducing agent. PomA was detected via western blotting using the anti-PomA
538 antibody. In the right side, the periplasmic loop regions of the *C. jejuni* (Cj) stator structure
539 (PDB ID: 6YKM) is shown by the ribbon model and the corresponding residues of *Vibrio*
540 L22C and T33C mutations of PomA were shown in blue with the ball-and-stick model. The
541 MotB part corresponding to PomB is shown in light blue. (B) *Vibrio pomAB* cells harboring
542 the same plasmids as (A) were inoculated in soft agar plates (VPG 0.25%) with 0.02%
543 arabinose and incubated at 30 ºC for 5 h. (C) Proteins extracted from *Vibrio pomAB* cells
544 harboring pHFAB-based plasmid with the mutations, 1: *pomA-L22C*, *T33C* (L22C&T33C), 2:
545 *pomA-L22C*, *T33C, K64P* (L22C&T33C+K64P), 3: *pomA-L22C*, *T33C, F66S*
546 (L22C&T33C+F66S), 4: *pomA-K64P* (K64P), and 5: *pomA-F66S* (F66S) were separated
547 using SDS-PAGE in the absence of a reducing agent. PomA was detected via western blotting
548 using the anti-PomA antibody. (D) *Vibrio pomAB* cells harboring the same plasmids as (C)
549 were inoculated in soft agar plates (VPG 0.25%) with 0.02% arabinose and incubated at 30 ºC
550 for 24 h.
551
552 **Fig. 7. Possible function of the CI region in loop$_{2\text{-}3}$ of *Vibrio* PomA.**
553 (A) Electrostatic potential map was estimated. (B) The structure of the Cj stator was shown
554 by the ribbon model. The regions corresponding to G53-A70 of PomA and the B subunit are
555 shown by blue and light blue, respectively. The red and the green indicate the α helix regions

556 and the TM3 or TM4 region close to the CI helix, respectively. (C) The corresponding region
557 of G53-A70 in (B) is expanded. The residues of MotA corresponding to K64 or F66 and
558 K203 of PomA are shown by the ball-and-stick model in black, and the space-fill model in
559 yellow, respectively.

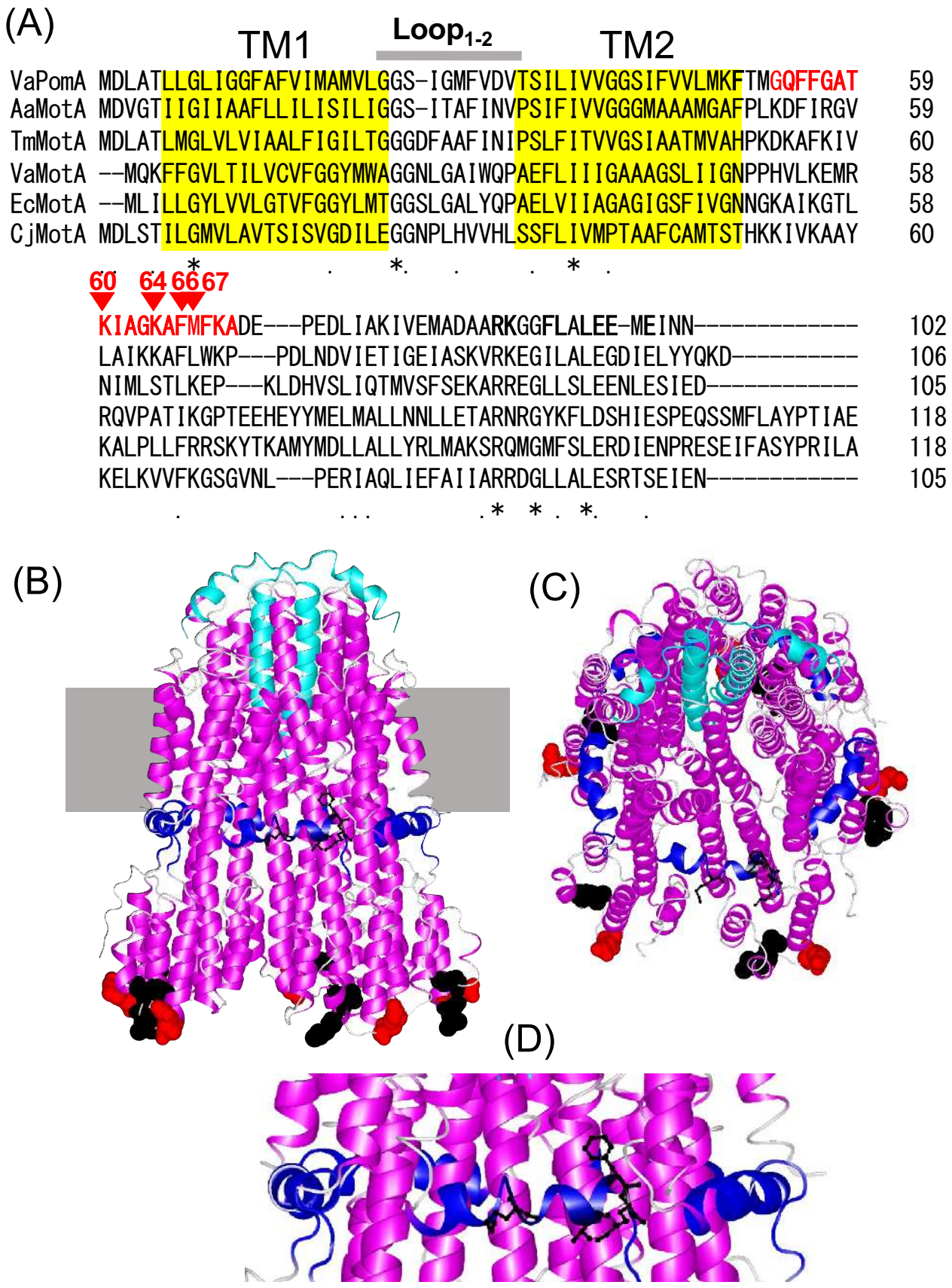
(A)
TM1
Loop1-2
TM2
VaPomA MDLATLLGLIGGFAFVIMAMVLGGS-IGMFVDVTSILIVVGGSIFVVLMKFTMGQFFGAT 59
AaMotA MDVGTIIGIIAAFLLILISILIGGS-ITAFINVPSIFIVVGGGMAAAMGAFPLKDFIRGV 59
TmMotA MDLATLMGLVLVIAALFIGILTGGGDFAAFINIPSLFITVVGSIAATMVAHPKDKAFKIV 60
VaMotA --MQKFFGVLTILVCVFGGYMWAGGNLGAIWQPAEFLIIIGAAAGSLIIGNPPHVLKEMR 58
EcMotA --MLILLGYLVVLGTVFGGYLMTGGSLGALYQPAELVIIAGAGIGSFIVGNNGKAIKGTL 58
CjMotA MDLSTILGMVLAVTSISVGDILEGGNPLHVVHLSSFLIVMPTAAFCAMTSTHKKIVKAAY 60
60 64 66 67
KIAGKAFMFKADE---PEDLIAKIVEMADAARKGGFLALEE-MEINN---------- 102
LAIKKAFLWKP---PDLNDVIETIGEIASKVRKEGILALEGDIELYYQKD---------- 106
NIMLSTLKEP---KLDHVSLIQTMVSFSEKARREGLLSLEENLESIED---------- 105
RQVPATIKGPTEEHEYYMELMALLNNLLETARNRGYKFLDSHIESPEQSSMFLAYPTIAE 118
KALPLLFRRSKYTKAMYMDLLALLYRLMAKSRQMGMFSLERDIENPRESEIFASYPRILA 118
KELKVVFKGSGVNL---PERIAQLIEFAIIARRDGLLALESRTSEIEN---------- 105
(B)
(C)
(D)

Fig. 1

(A)

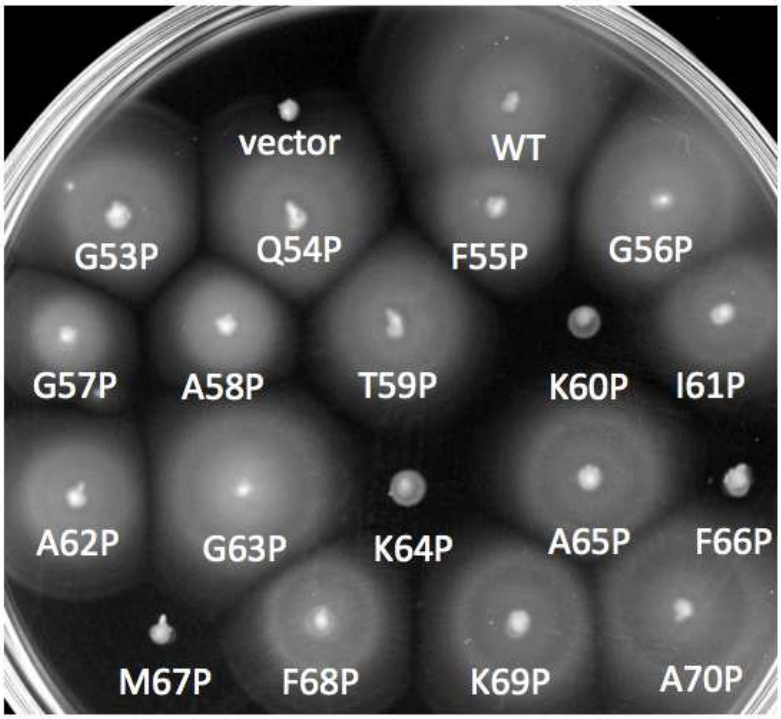
vector
WT
G53P
Q54P
F55P
G56P
G57P
A58P
T59P
K60P
I61P
A62P
G63P
K64P
A65P
F66P
M67P
F68P
K69P
A70P

(B)

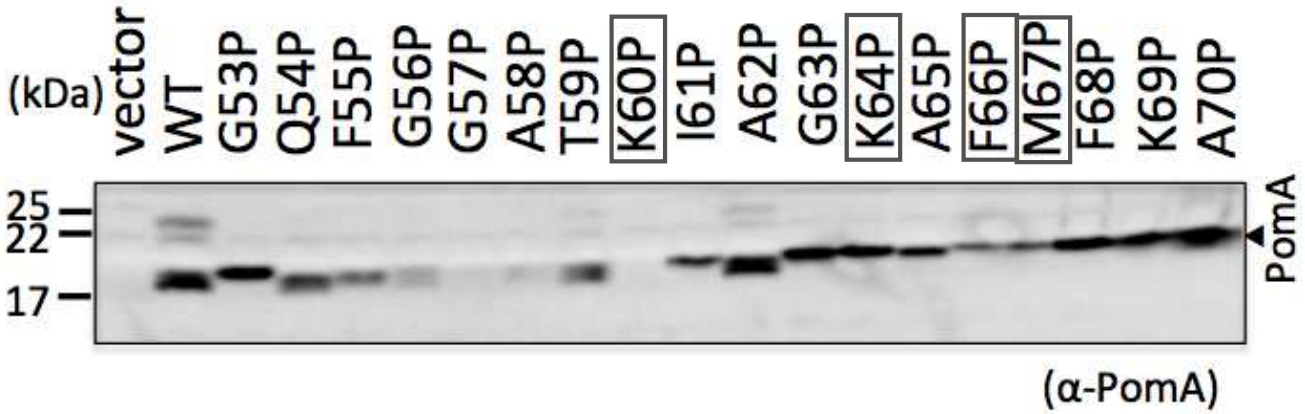
(kDa)
vector
WT
G53P
Q54P
F55P
G56P
G57P
A58P
T59P
K60P
I61P
A62P
G63P
K64P
A65P
F66P
M67P
F68P
K69P
A70P
25
22
17
PomA
(α-PomA)

Fig. 2

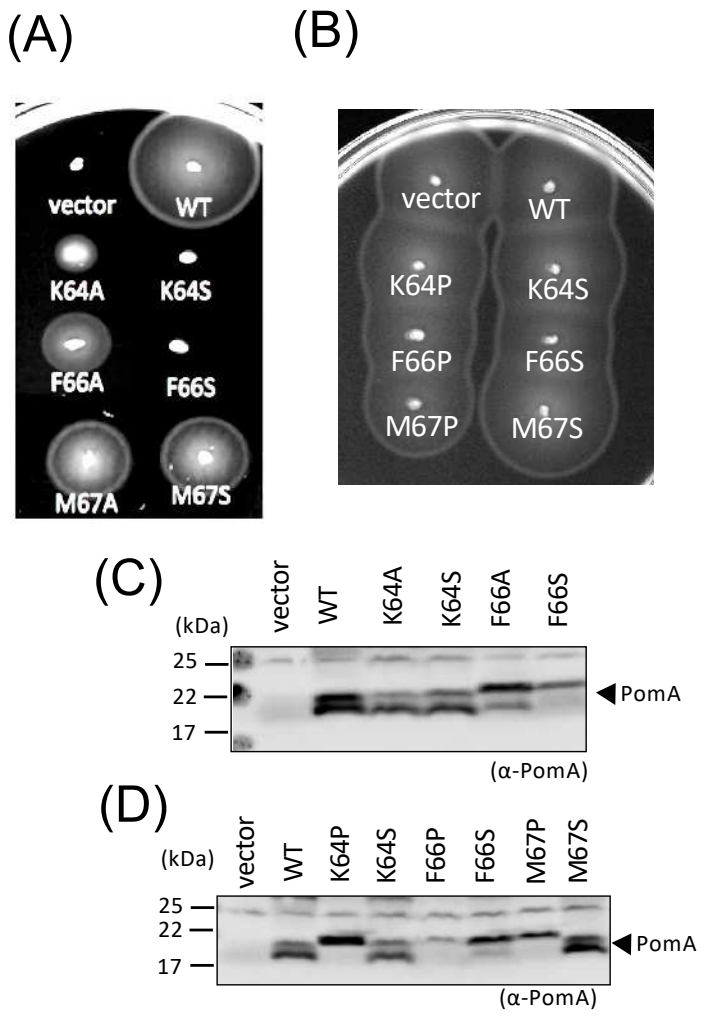
(A)
vector
WT
K64A
K64S
F66A
F66S
M67A
M67S
(B)
vector
WT
K64P
K64S
F66P
F66S
M67P
M67S
(C)
(kDa)
vector
WT
K64A
K64S
F66A
F66S
25
22
17
PomA
(α-PomA)
(D)
(kDa)
vector
WT
K64P
K64S
F66P
F66S
M67P
M67S
25
22
17
PomA
(α-PomA)

Fig. 3

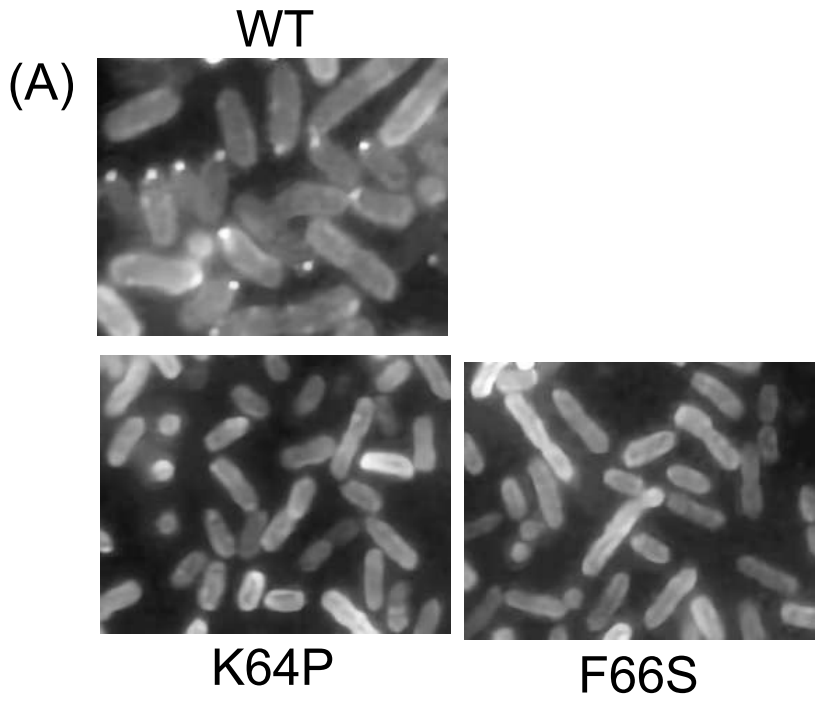
(A)
WT
K64P
F66S

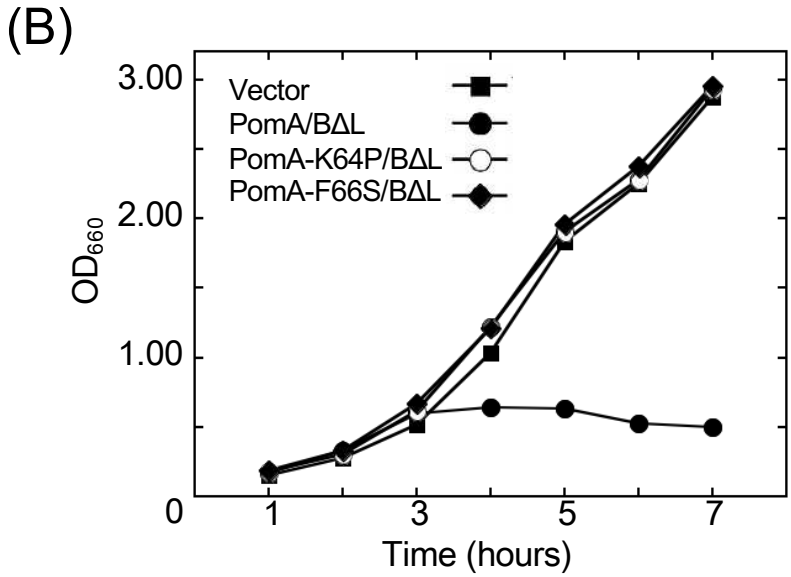
(B)
3.00
2.00
1.00
0
OD660
Vector
PomA/BΔL
PomA-K64P/BΔL
PomA-F66S/BΔL
1
3
5
7
Time (hours)

Fig. 4

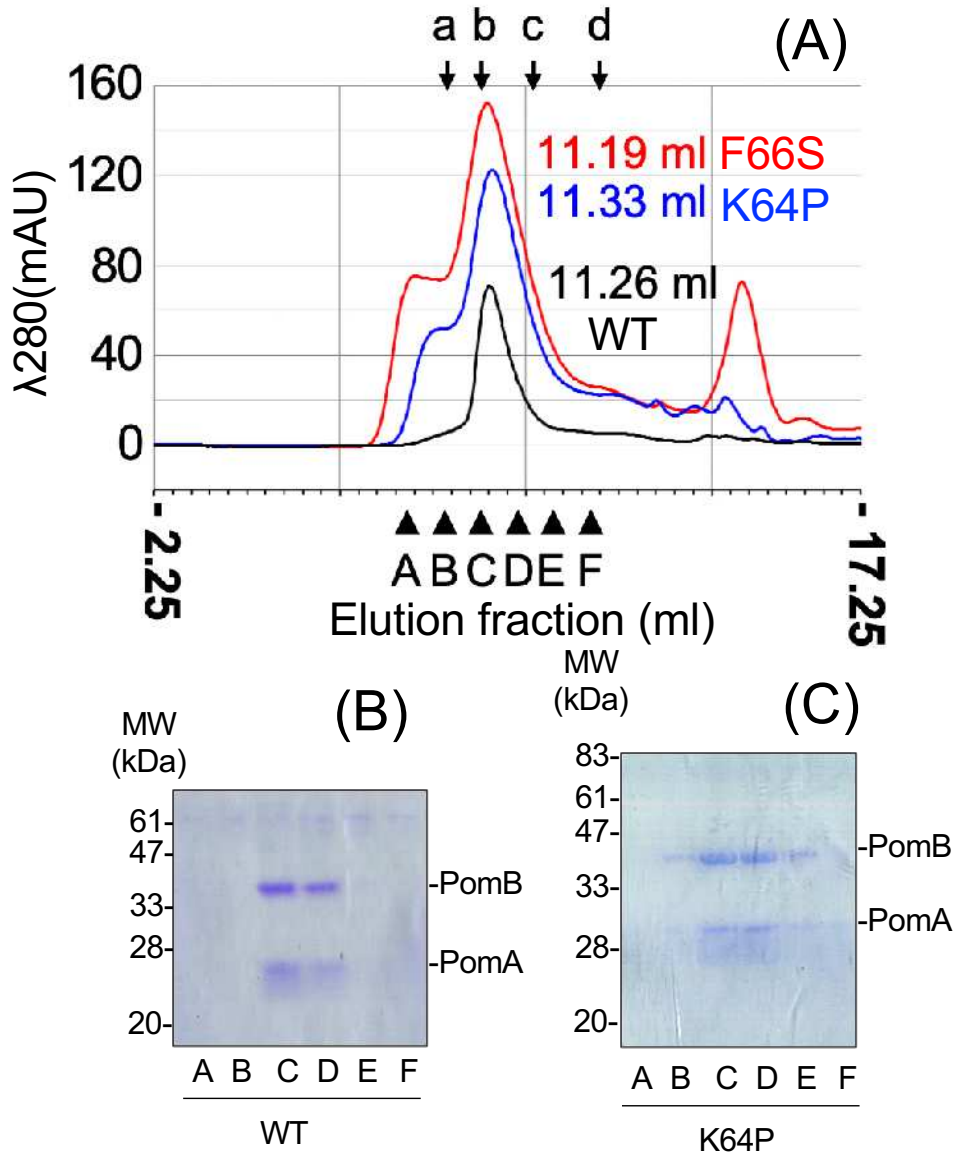
(A)
a b c d
160
120
80
40
0
λ280(mAU)
11.19 ml F66S
11.33 ml K64P
11.26 ml
WT
- 2.25
- 17.25
A B C D E F
Elution fraction (ml)
(B)
MW
(kDa)
61-
47-
33-
28-
20-
-PomB
-PomA
A B C D E F
WT
(C)
MW
(kDa)
83-
61-
47-
33-
28-
20-
-PomB
-PomA
A B C D E F
K64P

Fig. 5

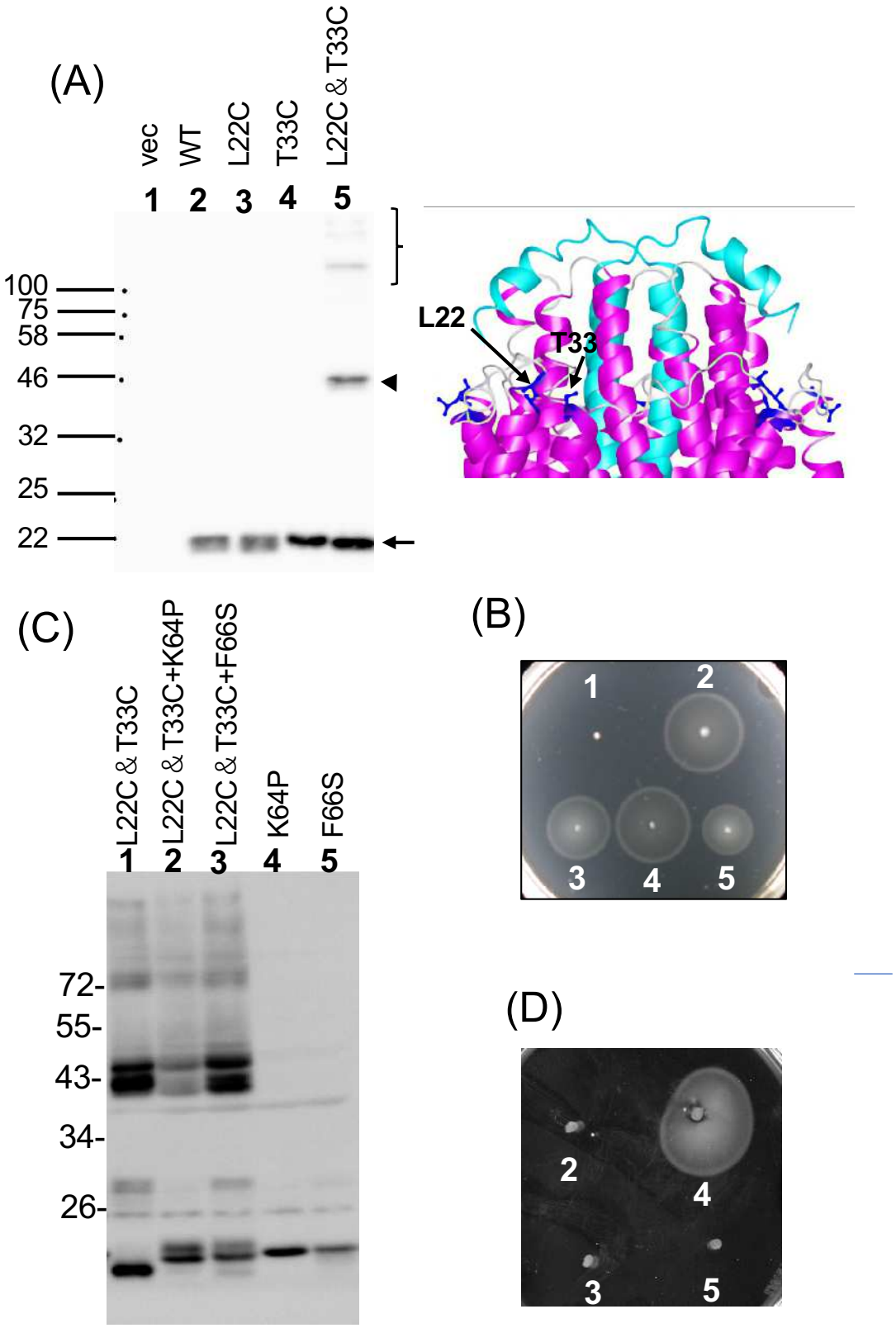
(A)
vec
WT
L22C
T33C
L22C & T33C
1
2
3
4
5
100
75
58
46
32
25
22
L22
T33
(B)
1
2
3
4
5
(C)
L22C & T33C
L22C & T33C+K64P
L22C & T33C+F66S
K64P
F66S
1
2
3
4
5
72-
55-
43-
34-
26-
(D)
2
4
3
5

Fig. 6

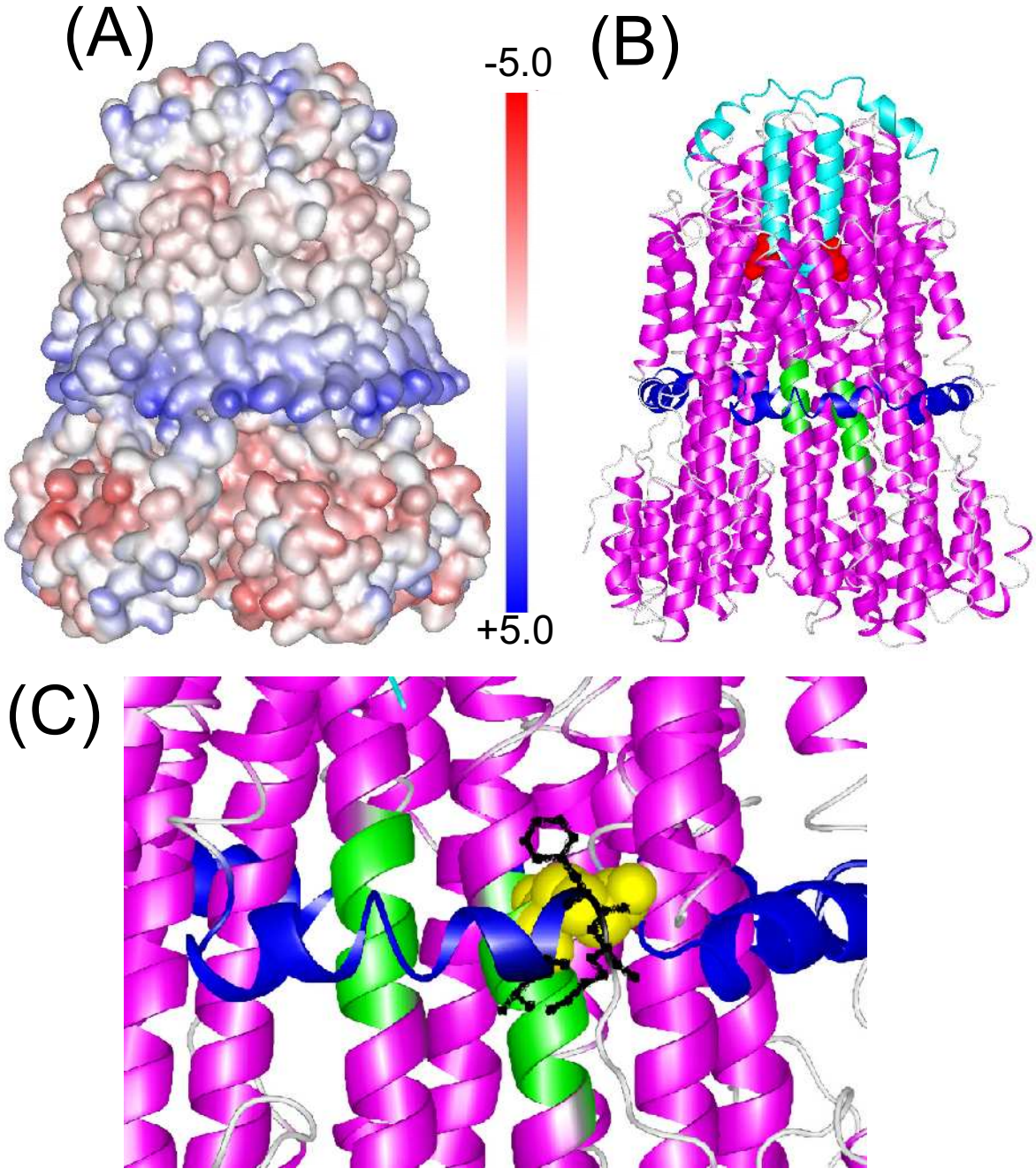

Fig. 7

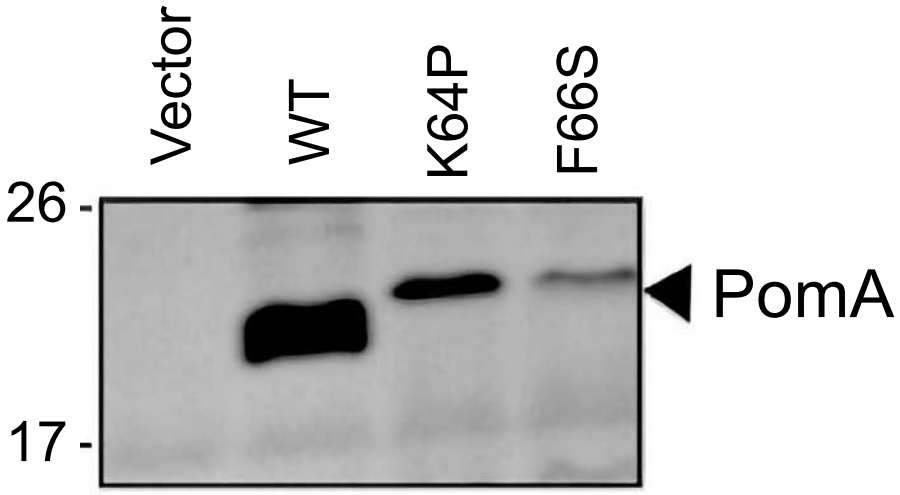

Fig. S1. Protein expression of PomA-K64P and F66S mutations with PomBΔL. (A) *E.coli* DH5α cells harboring the pHFAB-WT and pTSK37-based (PomBΔL) plasmids with the *pomA* mutations were grown to the mid-log phase. The proteins of the cells were then separated using sodium dodecyl sulfate-polyacrylamide gel (SDS-PAGE) and detected via western blotting using anti-PomA antibody

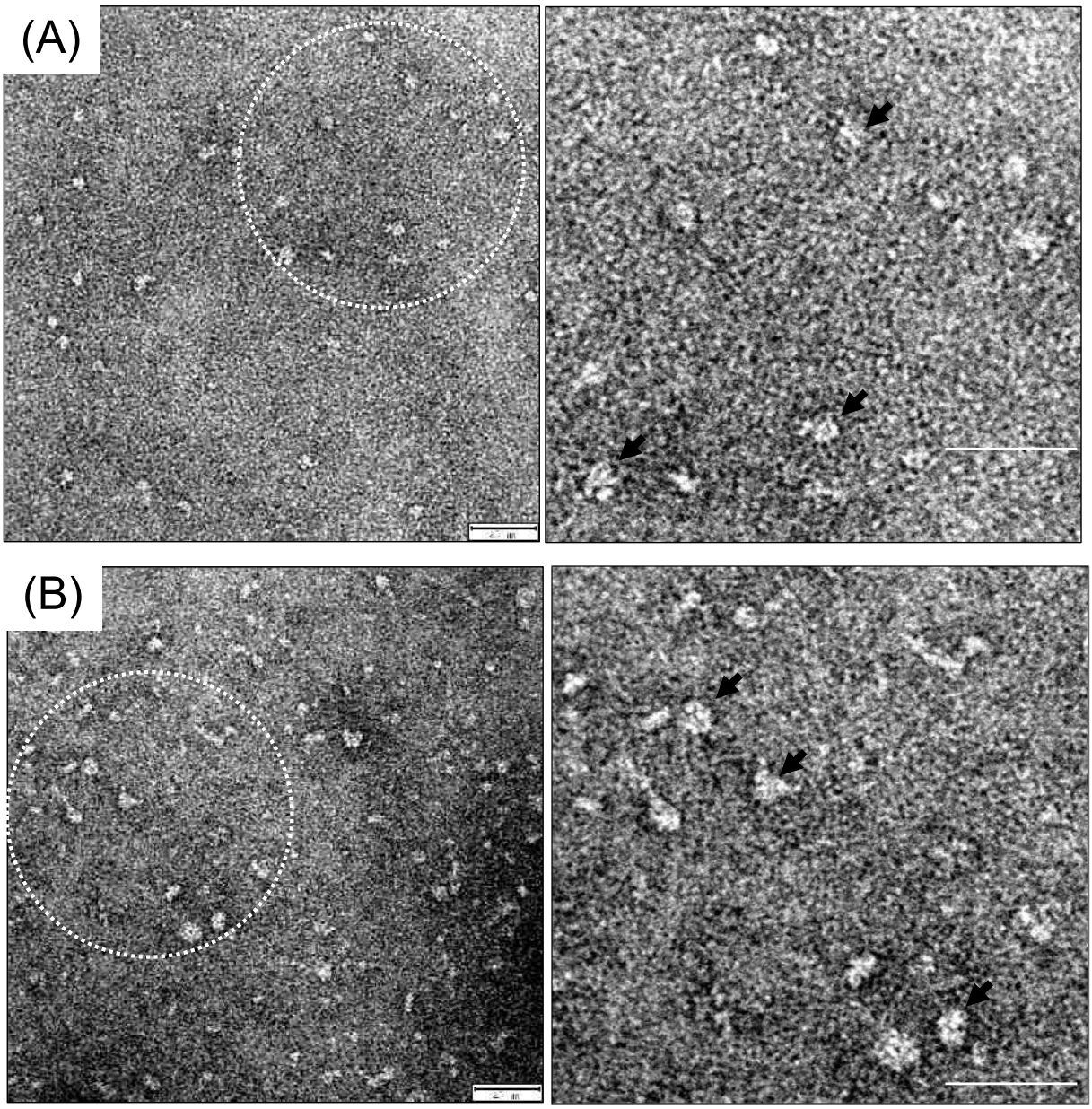

Fig. S2. Electron microscopic observation of the stator complex. The stator expressed in *Escherichia coli* cells by pColdIV-*pomA-pomB-his6* plasmid with wild-type (WT) PomA (A) or the F66S mutation (B) and purified by affinity chromatography using hexa-histidine tag was subjected to size exclusion chromatography. The purified stator complexes were observed with an electron microscope with negative staining. The right panels show the 2x magnified region of the white dash lines in the left panels. Some stators were indicated by arrows. Scale bars indicate 40 nm.

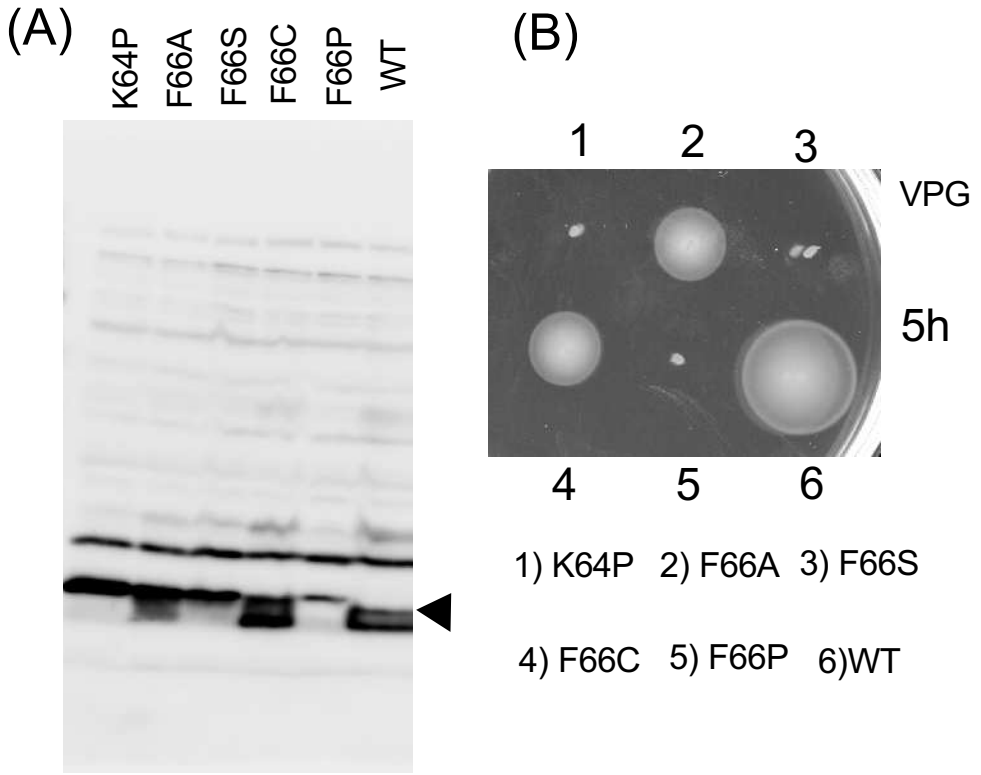

Fig. S3. Profiles of PomA mutations. (A) Proteins extracted from *Vibrio* NMB191 cells containing the pHFAB (WT) and pHFAB-based plasmids with the pomA-F66A (F66A), pomA-F66S (F66S), pomA-F66C (F66C), pomA-F66P (F66P), and pomA-K64P (K64P) mutations were separated by sodium dodecyl sulfate-polyacrylamide gel (SDS-PAGE) and detected by western blotting using the anti-PomA antibody. (B) NMB191 cells harboring the same plasmids as (A) were inoculated in soft agar plates (VPG 0.25%) with 0.02% arabinose and incubated at 30 ºC for 6 h.

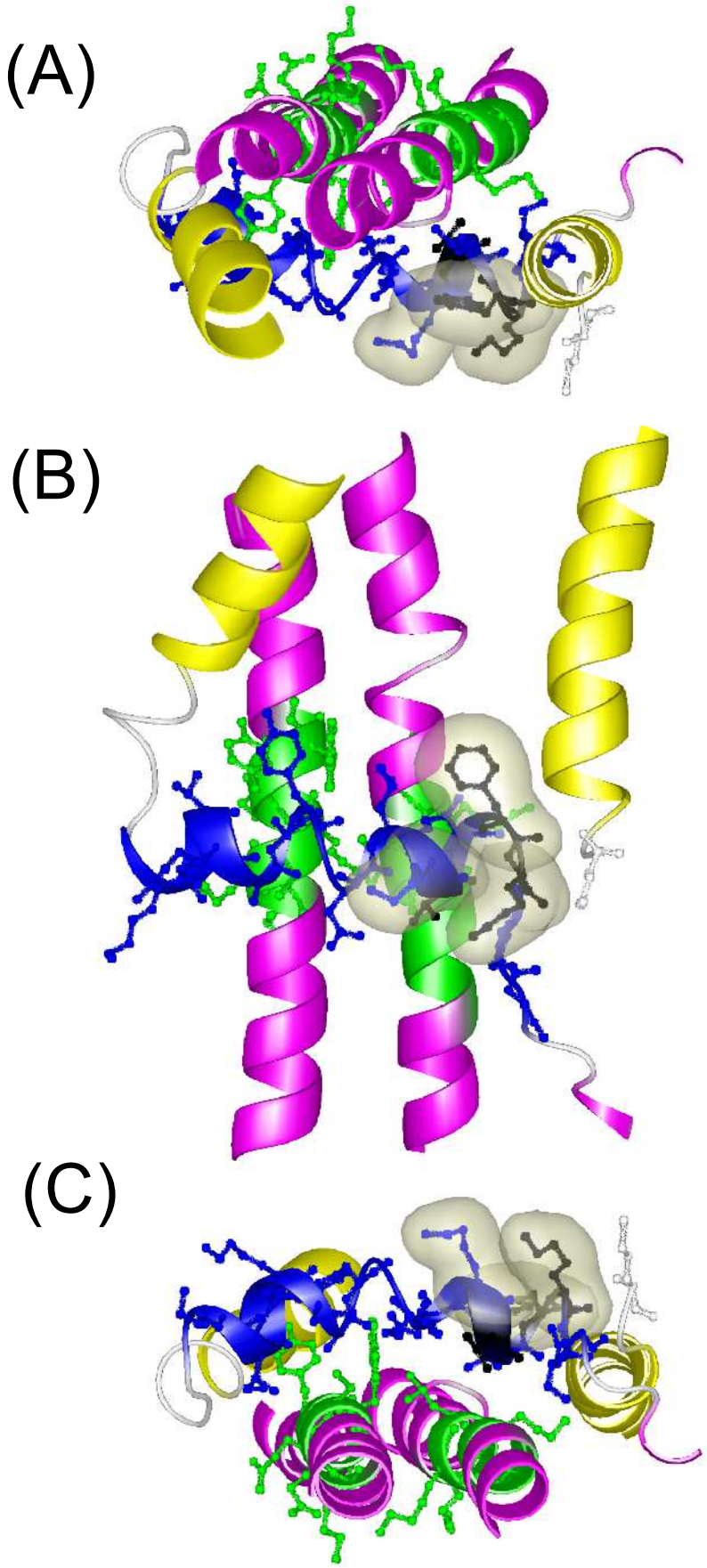

Fig. S4. The model of the cytosolic interface (CI) helix region. The structure of the *Campylobacter jejuni* (Cj) stator near the CI helix region was shown by the ribbon model. The residues corresponding to K64, F66, and M67 are shown by the ball-and-stick model in black with Van der Waals surface. The CI region of MotA corresponding to PomA is shown in blue. The regions of TM3 and TM4, which are close to the CI helix region are shown in green. TM1 and TM2 are shown in yellow.

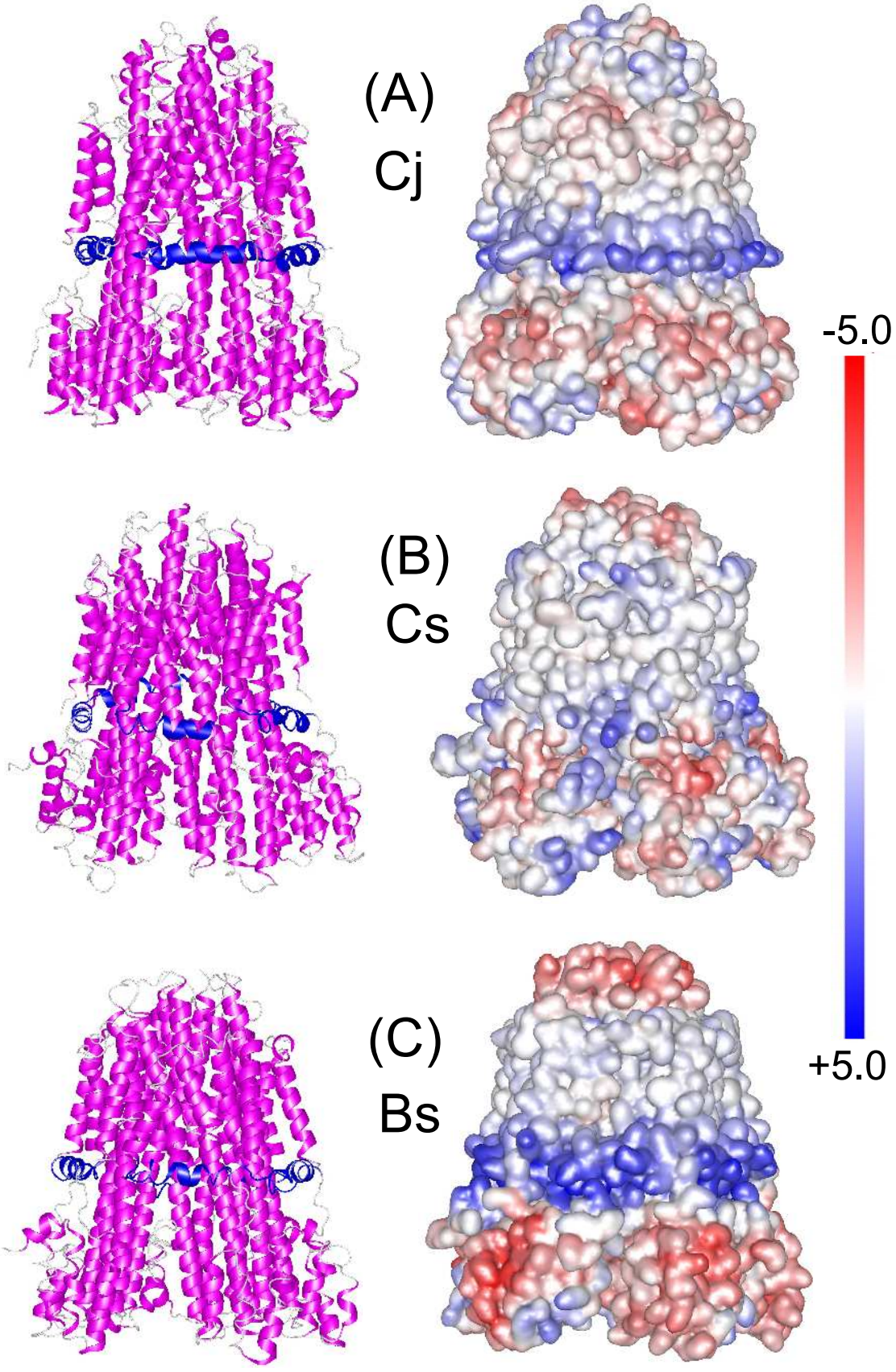

Fig. S5. The electrostatic potential map by surface modeling (right) and the ribbon model (left) of the structures of Cj stator (PDB ID: 6YKM) (A), *Clostridium sporogenes* (Cs) stator (PDB ID: 6YSF) (B), and *Bacillus subtilis* (Bs) stator (PDB ID: 6YSL) (C) are shown. The CI region of MotA by ribbon model is shown in blue.